eprints@whiterose.ac.uk
https://eprints.whiterose.ac.uk/

Quartz crystal microbalance as a device to measure the yield stress of colloidal suspensions

Johannes A. Botha[1], Wei Ding[1], Timothy N. Hunter[1], Simon Biggs[2], Graham A. Mackay[3], Robin Cowley[4], Simon E. Woodbury[5] and David Harbottle*[1]

[1] School of Chemical and Process Engineering, University of Leeds, UK
[2] School of Chemical Engineering, The University of Queensland, Brisbane, Qld 4072, Australia
[3] NNL Workington Laboratory, Cumbria, UK
[4] Sellafield Limited Analytical Services, Sellafield, Cumbria, UK
[5] NNL Central Laboratory, Sellafield, Cumbria, UK

* D.H., E-mail: d.harbottle@leeds.ac.uk, T: +44(0) 113 343 4154

Abstract

The application of quartz crystal microbalance (QCM) as a device to measure the rheology of colloidal suspensions has been studied. Using a commercial dip-probe QCM, the yield stress of magnesium hydroxide suspensions has been correlated to the resonance properties of a 5 MHz AT-cut quartz sensor. A stable resonance baseline was first established in air before submerging the sensor into the colloidal suspension. The response of the sensor resistance was shown to correlate to changes in the suspension yield stress, while the frequency response was found to result from more complex contact mechanics and suspension viscoelasticity contributions. Since the QCM is a relatively simple technique with no mechanically moving parts, this approach offers the potential for rapid in situ rheology assessment.

Introduction

The UK nuclear industry is currently entering a phase of post operational clean out (POCO) to safely remove and store legacy wastes which have accumulated over several decades of nuclear power generation. A particular concern for the UK is the legacy sludge waste which has been stored in open air ponds and silos and now needs to be retrieved for further interim storage or ultimate disposal. To ensure the safe recovery of the wastes, design guides for sludge retrieval

will be proposed based on the physical and chemical properties of the materials to be recovered. Understanding the rheology of the legacy sludge, along with its modification during handling is therefore of great importance. However, conventional rheometer techniques are often unsuitable due to issues of sample handling (radioactivity and methods of extraction), and the requirement to frequently collect data in confined spaces. With its simple design, small size and no mechanical parts, a quartz crystal microbalance (QCM) has the potential to directly measure rheology in challenging environments.

In its standard configuration, a QCM consists of a piezoelectric AT-cut quartz sensor with electrodes coated on each surface. Applying an oscillating electric field across the piezoelectric sensor generates an internal mechanical stress that vibrates the sensor[1]. Interpretation of the vibrational motion reveals the viscosity-density product of the deposited material from which other physical properties such a deposited film thickness and viscoelasticity can be determined[2-6].

The baseline data includes QCM resonance frequency and motional resistance. The resonance frequency is often quoted due to the simplicity of the Sauerbrey equation (Eq. 1) which provides a simple conversion of resonance frequency shift to deposited mass:

$$\Delta f = -\frac{2f_0^2 \Delta m}{A\sqrt{\rho_q \mu_q}} \tag{1}$$

where Δf is the measured frequency shift, f_0 is the fundamental frequency, Δm is the mass change, A is the sensor area, ρ_q is the density of quartz sensor (2.648 g cm^{-3}), and μ_q is the shear modulus of quartz sensor (2.947 x 10^{11} g cm.s^{-2}).

While a Sauerbrey conversion is often useful, the underlying principle as an extension of the resonating sensor is only truly valid when the added mass satisfies: i) no slip, ii) rigid deposition, and iii) even deposition on the sensor surface[2].

Nomura and Bruckenstein demonstrated the stable resonance of QCM when one surface of the sensor was intimately in contact with a bulk liquid[7-9]. Gordon-Kanazawa-Mason[3, 10-11] derived a simple relationship correlating the change in resonance frequency to changes in the density and viscosity of a non-adsorbing fluid (Eq. 2):

$$\Delta f = -f_{0*}^{\frac{3}{2}}(\frac{\rho_L \mu_L}{\pi \rho_q \mu_q})^{1/2} \tag{2}$$

where f_{0*} is the fundamental resonance frequency, and ρ_L and μ_L are the absolute density and viscosity of the fluid, respectively. More recently, studies based on the Mason equivalent circuit theory[12] or the Voigt-Voinova theory[13] have demonstrated the applicability of QCM to measure the viscoelastic properties of bulk fluids and deposited layers on the sensor surface.

While those fundamental studies highlight the great potential of QCM when investigating solid, liquid and gaseous systems, until recently solid-liquid systems had received very little attention; in particular particle suspensions. The interaction of particles and the QCM sensor has been considered in detail by Johannsmann and co-workers[6, 14], where the Mason model has been suitably modified to include point-contact loads that are relevant to non-uniform loads such as deposited particles on the resonating sensor. Of the few studies considering QCM and particles, other applications include i) measuring the particle concentration by drying suspensions onto the sensor[15] and ii) detecting particle deposition onto a heterogeneous surface,[16-17] with the resonance properties correlated to the colloidal forces acting between the resonating sensor and suspension. When studying particle systems, researchers have reported positive frequency shifts during mass deposition, which is contrary to the mass deposition theories described by Sauerbrey and Voigt-Voinova[18-20].

Dybwad and Pomorksa[20-21] developed a model termed the 'coupled resonance model' to account for such interesting behaviour. The model states that for a sphere in contact with a resonating sensor of angular frequency, ω, the sphere will adopt its own resonance of angular

frequency, $\omega_s = (\kappa/m)^{1/2}$, where κ is the contact stiffness and m the particle mass[20-21]. The contact stiffness is a function of both tangential and normal load contributions, although for a 5 MHz sensor the contact stiffness is strongly influenced by the normal oscillatory load due to the flexural contributions to the displacement pattern. If the sphere is small and the particle contact with the resonating sensor is sufficiently stiff, the condition $\omega_s \gg \omega$ holds true and 'inertial loading' occurs where the mass of the sphere reduces the sensor resonance frequency, i.e. Sauerbrey behavior [2, 20-21]. If the sphere is large however (typically > 1 µm) and is weakly bound to the sensor, the condition $\omega_s \ll \omega$ holds true and the resonance frequency of the sensor increases, described as 'elastic loading'[20-21]. Pomorska et al. performed finite element calculations on relevant systems and concluded that this phenomena is plausable in liquid phase media, where the resonance frequency of the sensor is dependent on the strength of the sphere-sensor contact rather than the adsorbed mass[20].

The objective of the current study is to extend the application of QCM and correlate the frequency and resistance responses to changes in the rheology of particle suspensions, i.e. the shear yield stress. The measurement approach is quite simple and involves measuring the frequency and resistance shifts from the baseline resonance in air to the steady-state values once submerged into the test material. In particular, samples of two different types of magnesium hydroxide were investigated, as similar materials are thought to represent the major fractions of corroded fuel canister wastes, present in various nuclear legacy ponds and silos in the UK[22].

Materials and Methods

Materials: Two magnesium hydroxide ($Mg(OH)_2$) samples were used as model test materials relevant to legacy nuclear waste in the UK. The first test material Versamag A was supplied by Rohm and Hass and the second test material Versamag B (sample labelling used throughout)

was supplied by Martin Marietta. Both samples were chosen due to their varied magnesium oxide (MgO) contents leading to differences in aging behavior, see discussion below. The pH of all suspensions was maintained at pH 10.2 due to the natural buffering of the system, which corresponded to conditions close to the particle isoelectric point ($pH\ 10.2,\ \zeta = -7 \pm 4\ mV$). Both particle types were used as received and dispersed in deionised water with a resistivity of 18 MΩ.cm.

Sample aging: 80 g Versamag (A or B) was added to 120 g deionised water (solid content = 22 vol%) in a 250 mL glass beaker and hand mixed for 15 min until the suspension resembled a smooth paste. The suspension was left undisturbed for 5 min before measuring the yield stress and QCM response (separate samples). The objective of the aging tests was to measure the time-dependent changes in the suspension yield stress between 0 and 70 h. The suspension volume fraction was chosen such that the particle concentration exceeded the gelling concentration[23-24] (Fig. S1), hence no suspension consolidation would occur during sample aging. To avoid yield stress changes due to sample drying, a thin layer of mineral oil ($\rho = 0.84$ g/cm^3) was gently pipetted onto the suspension (following immersion of the QCM sensor), before finally sealing the glass beaker with Parafilm.

The shear yield stress was measured using an AMETEK Brookfield DV-II+ Pro Viscometer with a four blade vane (H = 43.33 mm, D = 21.67 mm). The vane was gently lowered into the sediment to a pre-determined height and rotated at 1 rpm for 2 min, with the motor torque continuously measured. At the yield point the suspension begins to flow and the measured torque decreases. The shear yield stress (τ_y) can be calculated from the maximum torque and vane dimensions as follows[25-26]:

$$\tau_y = \left.2T_{(max)}\middle/\pi D^3\left(\frac{H}{D}+\frac{1}{6}\right)\right. \tag{3}$$

where $T_{(max)}$ is the maximum torque, D is the vane diameter, and H is the vane height. To minimize any wall effects, the vane-to-cylinder ratio equalled 1:3.5, and the glass beaker was held in place using a clamp to ensure no sample rotation during the measurement.

Equivalent time-dependent studies were completed using a Stanford Research Systems (SRS) QCM 200, see Fig. S2. A 5 MHz AT-cut gold coated quartz sensor (d = 25.4 mm) was cleaned by sonication in 2 vol% Decon-90 solution for 5 min and rinsed thoroughly with deionised water prior to drying under a stream of N_2 gas. The cleaned sensor was then mounted in the QCM holder and left to resonate in air for approximately 30 min. The QCM compensation was adjusted to null the capacitance ensuring that the frequency and resistance values reflected the true resonant properties of the sensor. A stable resonance frequency and resistance was achieved when the sensor responses were within the limits of 2 Hz/h and 0.5 Ohm/h, respectively.

With a stable baseline the QCM probe was gently submerged into the suspension and agitated to enhance the sensor-suspension contact. The QCM probe was repeatedly agitated until the frequency and resistance values of the sensor stabilized, thus confirming good contact between the QCM sensor and particle suspension. The QCM compensation was then re-adjusted to null the capacitance. To avoid any sensor drift due to thermal fluctuation, the sample beaker was submerged in a water bath that was heated using a hot plate. A temperature probe was immersed in the suspension to maintain the temperature at 30 °C. Long term (70 h) stability of the QCM sensor was first verified by conducting a time-dependent measurement in water, see Fig. 4.

Solids concentration: With minimal time-dependent aging, Versamag B was chosen to study the effect of solids concentration on the shear yield stress and QCM response. A stock suspension of 44.2 vol% Versamag B was prepared and left to hydrate for two weeks. The stock suspension was prepared in a sealed container and periodically agitated (hand stirring)

before diluting the suspension to the desired solids concentration for testing. All test samples were mixed until homogenous and used within three days following hydration.

The same method for measuring the shear yield stress was followed. However, the range of shear yield stresses was broad, and thus to ensure that the maximum torque of the viscometer was not exceeded, two vane geometries of different dimensions were used: Vane 72 (H = 43.33 mm, D = 21.67 mm) for yield stresses between 0 Pa to ~ 40 Pa, and Vane 73 (H = 12.70 mm, D = 12.50 mm) for yield stresses > 45 Pa. Previous research has shown good agreement between shear yield stresses measured using different sized geometries in the crossover region [25, 27-29].

The QCM measurement protocol followed the method previously described. Since all measurements were completed within 30 min, sample drying was considered negligible in the absence of a thin oil layer.

Particle size distribution: A Malvern Mastersizer 2000 E (Malvern Instruments, UK) was used to measure the particle size distribution of both Versamag samples. Particle suspensions were prepared to 0.9 vol% and sonicated for 10 min. The particle size distribution and Scanning Electron Microscopy (SEM) images of Versamag A and B are shown in Fig. 1. The d_{50} for both samples is almost equivalent (~ 4 µm), although the Versamag B sample showed an observable shoulder towards the larger particle fraction leading to a d_{90} ~ 20 µm compared with d_{90} ~ 15 µm for Versamag A. Both samples had a d_{10} equal to 1.5 µm. SEM images of the two particles revealed a tabular plate-like crystal formation common to the Brucite crystal structure[30].
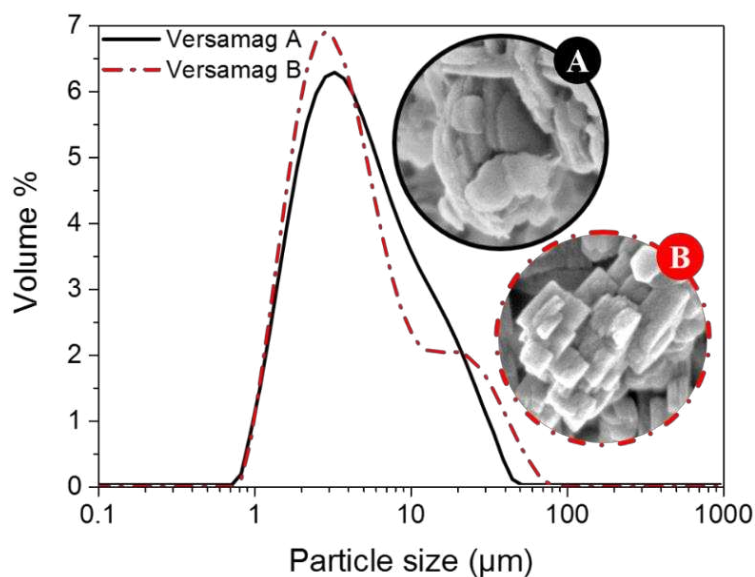
Figure 1. Particle size distribution and SEM images showing the physical appearance of aggregated (A) Versamag A and (B) Versamag B (circlet scale is 500 nm in diameter).

X-ray diffraction (XRD): Dried samples were disaggregated using a mortar and pestle and mounted in a PANalytical X'pert Powder X-ray diffractometer (pXRD), with Cu-Kα radiation ($\lambda = 0.15418$ nm) in the 2θ range of 10° - 65° with step size of 0.01˚. Lattice parameters for MgO (Periclase) (ICDD: 04-014-7440) and $Mg(OH)_2$ (Brucite) (ICDD: 04-011-5938) were obtained from the International Centre for Diffraction Data – Powder Diffraction File database (ICDD-PDF4+).

Intensity-normalised X-ray diffraction patterns for Versamag A and B are shown in Fig. 2. Both Versamag samples were predominantly composed of a crystalline hydrated $Mg(OH)_2$ phase (Brucite, ICDD 04-011-5938), comprising infinite stacked layers of Mg-O-Mg sheets. Some minor MgO-content (Periclase, ICDD 04-014-7440), a by-product of the manufacturing process, was also present in both samples, where the higher intensity-maxima of the Periclase [002]-reflection at ~ 43° 2theta (Fig 2. inset) indicates a higher apparent oxide content for Versamag A.
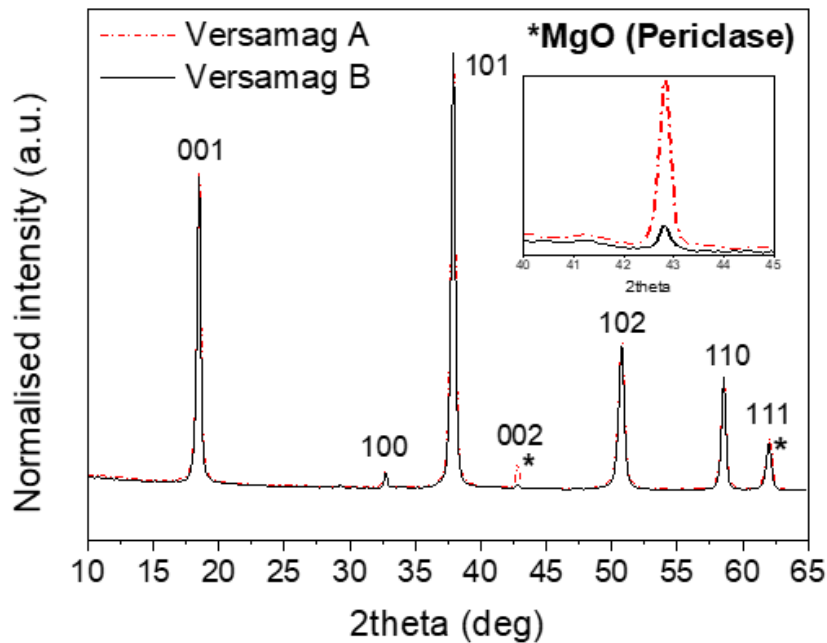
Figure 2. Intensity normalised X-ray diffraction patterns for Versamag A and B.

Thermogravimetric-Differential Scanning Calorimetry (TGA-DSC): Aliquots of the aged Versamag samples were extracted and quenched using propan-2-ol and allowed to dry. Samples were subsequently pulverised and inserted into 70 μL alumina crucibles (Mettler Toledo) of known mass and weighed. Dynamic thermogravimetric and calometric analyses were carried out using a TGA-DSC 1 (Mettler Toledo) under dry air (70:30 N_2:O_2 mix) at a flow-rate of 50 mL/s. The heating rate was set at 10 ℃/min and data was recorded between 250 ℃ and 450 ℃. Background scans using spent samples (pure MgO) were subtracted from mass loss data to account for air buoyancy effects.

The MgO content was determined by firstly calculating the molar amount of water lost between 250 – 450 °C. The mass of $Mg(OH)_2$ was then calculated through the degradation reaction $Mg(OH)_2 \rightarrow MgO + H_2O$ [31], with the theoretical $Mg(OH)_2$ mass then subtracted from the original sample mass to yield the MgO content. In addition, the enthalpy change per mole of $Mg(OH)_2$ was determined by integrating the peak obtained in the heat flow as the $Mg(OH)_2$ thermally decomposes (Fig. S3).

Results and Discussion

Sample aging: Vane viscometry was used to assess the time-dependent shear yield stress of Versamag A and B. The two Versamag samples exhibited different aging behaviour (Fig. 3) with the yield stress of Versamag A significantly increasing from ~50 Pa to ~300 Pa (~ 490% increase), showing rapid strengthening between t = 6 and 21 h, while Versamag B attained a maximum yield stress of ~73.5 Pa (~ 46% increase from ~50 Pa at t = 0) at 70 h aging. As previously discussed, aging effects due to sediment consolidation and/or sample drying can be considered negligible, with the sample aging dynamics more associated to the physicochemical properties of the two particle types, see later discussion.
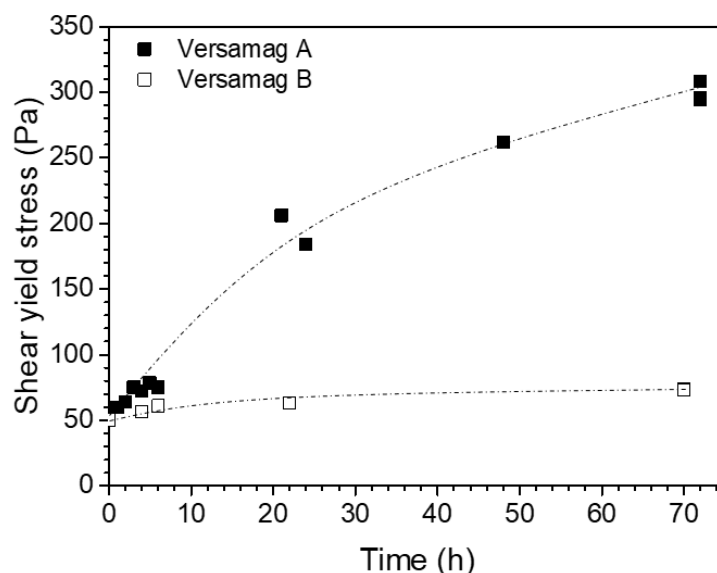

Figure 3. Time-dependent shear yield stress of 22 vol% Versamag A and B.

In situ QCM measurements confirmed the contrasting aging behaviour of Versamag A and B. The sensor resonance frequency (Hz) and resistance (Ohm) were measured (Fig. 4) with the QCM submerged in both Versamag suspensions. At t = 0, the measured frequency and resistance for both Versamag samples were almost equivalent, confirming comparable rheology for the freshly prepared samples (Fig. 3). However, during sample aging the sensor resonance frequency and resistance for Versamag A increased, with the sensor frequency

eventually exceeding the stable resonance frequency in air (i.e. when ΔF = 0 Hz). This behaviour is in contrast with the QCM response when submerged in Versamag B, where measured changes were significantly smaller. To verify that these changes in resonance frequency and resistance were not due to instabilities of the QCM sensor, we have also included a 70 h aging test for water only. With good temperature control (T = 30°C) throughout the experiment, neither the sensor resonance frequency nor resistance fluctuated, thus confirming the stability of the QCM sensor. The QCM responses were in good agreement with shear yield stress trends (Fig. 3), i.e. the QCM frequency and resistance were responsive to the increasing suspension yield stress.
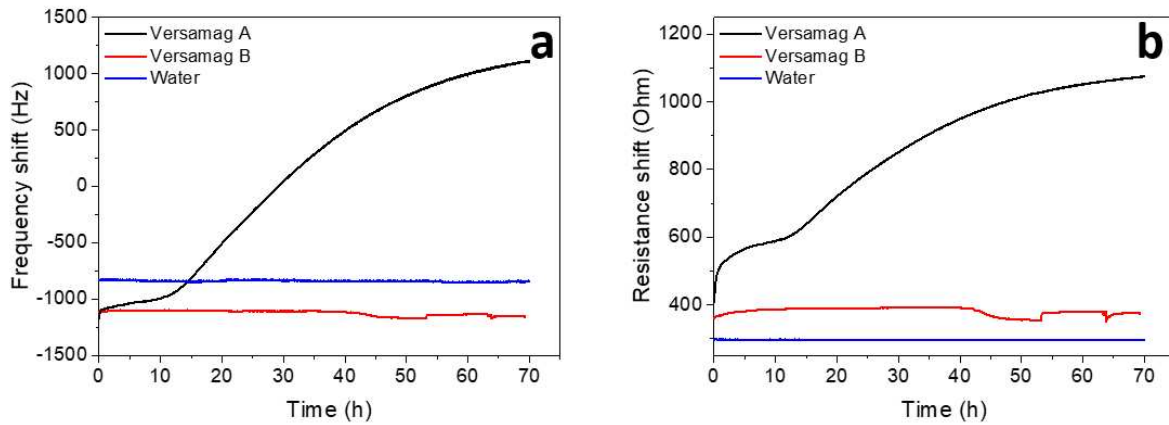

Figure 4. Time-dependent QCM air-to-sample (a) ΔF and (b) ΔR responses for Versamag A (black line), Versamag B (red line), and water only (blue line).

Further analysis of the Versamag A QCM data revealed a time-dependent response characterized by an approximately bilinear trend (Fig. 5). The resistance shift ΔR_1 (Ohm) can be transformed to a shift in half-bandwidth $\Delta\Gamma$ (Hz) using Eq. 4 [32]:

$$\Delta R + i\Delta f = \frac{A}{4\phi^2}\tilde{Z}_L = -i\frac{\pi}{16}\frac{Z_q^3}{Ae_{26}^2\rho_q^2 f_0^3}(\Delta f + i\Delta\Gamma) \tag{4}$$

where A is the active sensor area (m^2), Z_q the acoustic wave impedance (8.8 × 10^6 kg m^{-2} s^{-1}), e_{26} the piezoelectric stress coefficient (9.65 × 10^{-2} C m^{-2}), ρ_q the density of crystalline quartz

(2.65 g cm^{-3}) and f_0 the fundamental resonance frequency (5 MHz). Solving Eq. 4 leads to a simple conversion of $\Delta\Gamma \sim 2\Delta R_1$. The apparent differential loss tangent $\frac{\Delta\Gamma}{\Delta F}$ for Region I (t = 1 h to ~8.6 h) was 1.992 and for Region II (t = ~8.6 h to ~13 h) $\frac{\Delta\Gamma}{\Delta F} = 0.445$. A higher apparent differential loss tangent in Region I suggests that the measured mass is more lossy, since $\Delta\Gamma$ measures losses, while ΔF measures stiffness. Thus, the stiffness contribution dominates Region II as the suspension yield stress increases. Some non-linearity lies at the threshold between the two regions (Fig. 5, ΔF = ~-1000 to -750 Hz at ~16 h), indicating a non-steady-state transition from Region I to Region II. Since the particle and sensor zeta potentials were expected to remain constant (no change in pH or electrolyte concentration), these two regions highlight a two-stage aging process which most likely contributes to the increased suspension yield stress.
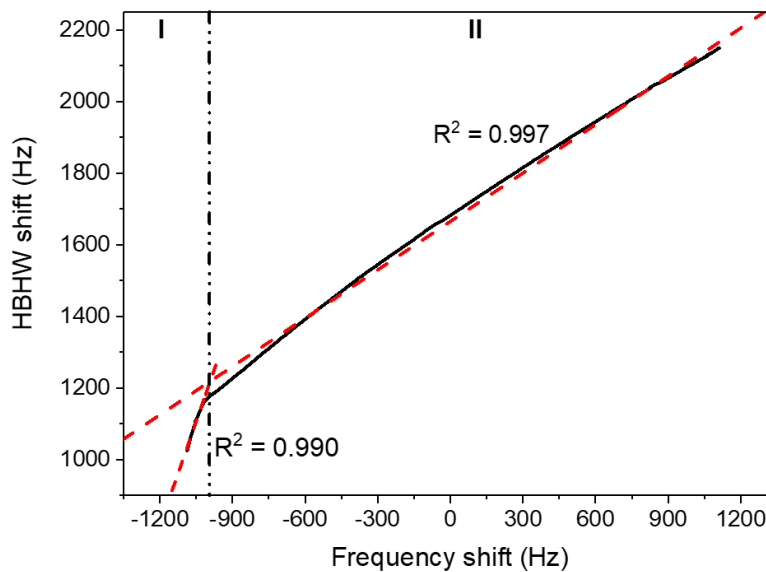
Figure 5. Apparent differential loss tangent ($\Delta\Gamma/\Delta F$) as a function of sample aging, suggesting the occurrence of a 2-stage aging process (sample: Versamag A).

XRD analysis (as previously shown in Fig. 2) revealed measurable differences in MgO content between Versamag A and B prior to aging. As MgO hydration to form Mg(OH)$_2$ is expected to occur in water, ex situ time-dependent-XRD was performed to verify this conversion with

the aging of Versamag A (Fig. 6a). To this end, 7 g samples of Versamag A were hydrated sacrificially for 0, 24, 48 and 70 h, before reactions were quenched by rinsing in 20 mL propan-2-ol, followed by air-drying for 12 h. X-ray diffractograms revealed a progressive reduction in the Periclase [002]-peak with increasing aging time (Fig. 6b), indicating significant dissolution, or conversion of Periclase (MgO) into Brucite ($Mg(OH)_2$). Using the Scherrer equation (K = 1)[33] to approximate the crystallite size for Brucite across multiple reflection peaks ([001], [100], [101], [102], [110], [111]), Versamag A showed little variation and the crystallite size was substantially smaller than that measured for Versamag B (Fig. 6c). Such small changes in crystalline size may preclude direct MgO to $Mg(OH)_2$ conversion from influencing the QCM response, instead an aggregation-dominated mechanism akin to oriented attachment or Ostwald ripening effects could be more influential[34].
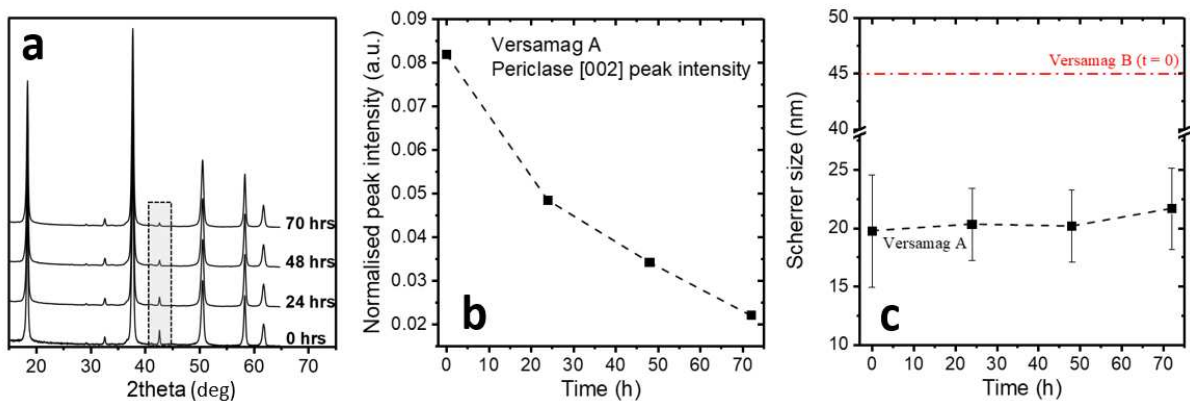

Figure 6. (a) X-ray diffraction patterns of Versamag A after sample aging for 0, 24, 48 and 70 h – shaded region represents the Periclase [002] peak. The Periclase [002]-peak intensity was normalized to the Brucite [101] maximum peak and plotted as a function of aging time (b). The calculated Scherrer crystallite size as a function of sample aging was compared with Versamag B at t = 0 (c).

The apparent two-stage hydration of Versamag A (Fig. 5) via the aggregation mechanism was further explored using ex situ thermal analysis of samples aged for t = 0, 4, 16, 24, 31, 48 and 72 h. The MgO contents for the fresh Versamag A and B samples were ~16.6 wt% and ~11.5

wt%, respectively, in good agreement with the qualitative assessment by XRD, see Fig. 2. The enthalpy associated with the decomposition (ΔH_d) of $Mg(OH)_2$ was determined from integrating the DSC heat-flux peaks, see Fig. S3. ΔH_d ranged between -45 and -80 kJ/mol of $Mg(OH)_2$, smaller than previously reported activation energies (E_a) for the dehydroxylation of $Mg(OH)_2$ (-80.75 to -98.74 kJ/mol [31, 35]), but larger than the dissociation enthalpy of sorbed water (-40.92 kJ/mol [36]), indicating that both hydrate-dissociation and dehydroxylation processes contribute to the dehydration of Versamag A and B. Hence, the observed two-stage aging (Fig. 5) may suggest a dissolution-precipitation reaction of $Mg(OH)_2$. When dispersed in water, MgO and smaller $Mg(OH)_2$ particles undergo increased rates of dissolution. As the aqueous solution becomes more saturated, precipitated $Mg(OH)_2$ may coat the MgO reactant, thus precipitation will exceed dissolution[37-38]. This enhances the number of bonds between particles, which stiffens the overall particle-particle network and increases the suspension yield stress (Fig. 3)[39-40].

Suspension concentration: The suspension shear yield stress can be increased by several orders of magnitude by increasing the solids concentration. The shear yield stress of Versamag B was firstly measured using the vane viscometer and corresponding measurements completed using the QCM. Fig. 7 confirms the exponential increase in shear yield stress with increasing solids concentration.[29]
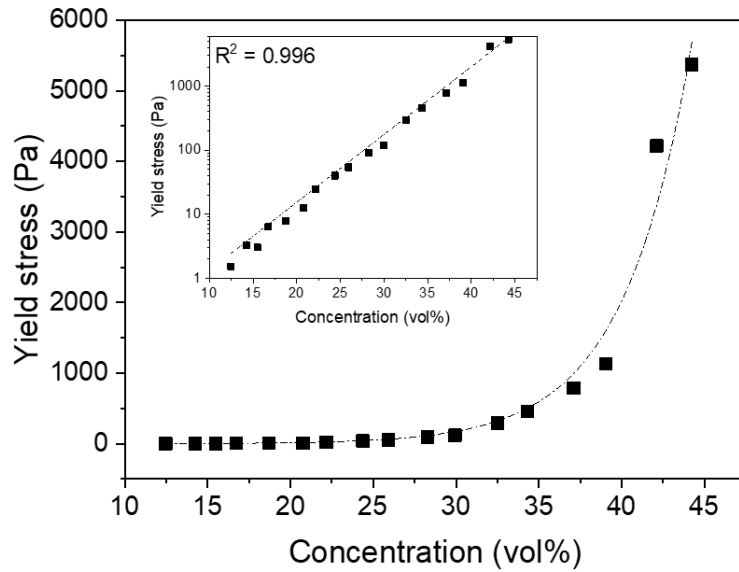
Figure 7. Shear yield stress of Versamag B suspensions as a function of the solids concentration. Data collected using the vane viscometer.

Complementary QCM tests were conducted (Fig. 8) to determine the QCM response as the suspension yield stress increased. The measured ΔR (Fig. 8a) also exhibited an apparently exponential response to changes in the suspension yield stress (Fig. 7), with the two data sets showing excellent agreement with a correlation coefficient $R^2 = 0.984$, see Fig. 8b. The motional resistance across the QCM circuit is a measure of the amount of energy required to oscillate the sensor. Therefore, as the suspension concentration is increased, the number of point contacts between the sensor and suspension is also thought to increase, thus providing greater resistance to the oscillating sensor. Such an effect may also be enhanced by the 'caging' of particles due to restrictions from their closest neighbours[41].
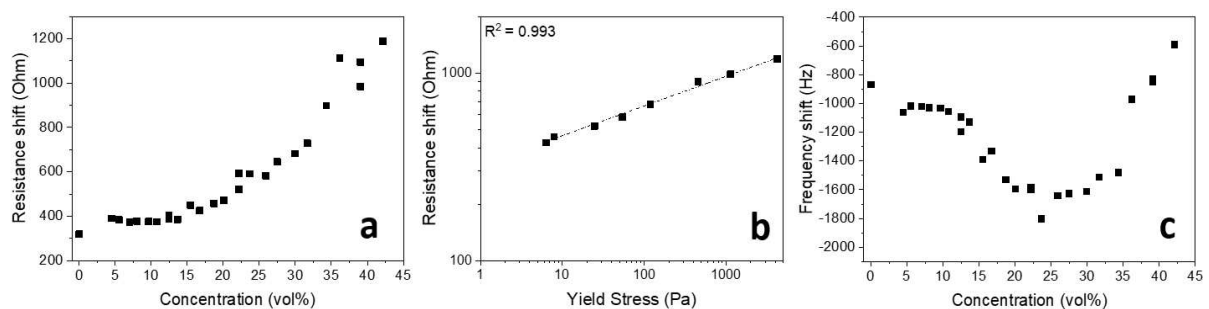
Figure 8. QCM ΔR (a), its correlation to suspension yield stress (b) and ΔF (c) responses for Versamag B as a function of solids concentration.

In the solids concentration range $5 - 43$ vol%, the frequency response (Fig. 8c) was less characteristic of the exponential increase in suspension shear yield stress. At lower solid concentrations ($5 - 12$ vol%), the measured $-\Delta F$ was shown to be almost independent of the increasing solids concentration. At these low concentrations, the suspension was below the gel point (Fig. S1), hence, a contiguous particle network throughout the suspension had not formed, and particles remained mobile relative to one-another. As such, the suspension loading on the resonating sensor remained constant due to the negligible suspension yield stress. The small decrease in frequency (~ 70 Hz) over the solids concentration range likely resulted from changes in the bulk fluid properties, i.e. small changes in the suspension density and viscosity.

In the solids concentration range ~ 12 to ~ 23 vol%, the QCM $-\Delta F$ response increased with increasing solids content. The solids concentration was now beyond the suspension gel point, hence a 3D contiguous network had formed, restricting particle mobility, and inducing an intermediary suspension yield stress ($\sim 2 - 30$ Pa). As the particle network in contact with the QCM sensor stiffens (i.e. increased yield stress), the QCM may detect the associated stiffening as an increase in the apparent mass loaded on the sensor[2], or as a stiffening viscoelastic medium[6]. Another factor that has not yet been explored, is the influence of the contiguous particle network on the shear wave penetration depth. For a 5 MHz sensor, the shear wave penetration depth (or viscous penetration depth) in water is ~ 250 nm (penetration depth $\delta = \left(\frac{2\mu_L}{\omega\rho_L}\right)^{1/2}$), with the penetration depth forming the measurement region[6]. With contacts between the sensor-particle and particle-particle, the pathway for dissipating energy is likely to vary from a simple viscous decay. As such, an increase in the shear wave penetration depth would result in increased 'mass sensing' and an overall increase in the air-sample $-\Delta F$.

With further increases in solids concentration (> 23 vol%) the suspension yield stress was observed to increase to several thousand Pa. In response, the air-to-sample frequency shift of the QCM sensor decreased, eventually measuring frequency shifts less than $\Delta F_{water} = -825$ Hz (i.e. no particles). At such high yield stresses the apparent mass detected by the QCM may now become large enough for the condition $\omega_S \ll \omega$ to be satisfied, resulting in a transition from inertial to elastic loading[2, 20-21]. Alternatively, we could also consider the frequency response to be governed by changes in the suspension viscoelasticity. Hence, an increase in the viscoelastic ratio of the suspension, storage modulus (elastic component) to loss modulus (viscous component), may lead to changes in the sensor resonance frequency (i.e. less negative shift) [6]. At present, it is not possible to exactly describe the mechanism(s) governing the measured frequency shifts, further work is ongoing.

Conclusions

A new technique to characterize the rheology of colloidal suspensions has been demonstrated. QCM is ubiquitously used to study kinetics, adsorbed/deposited film and bulk fluid properties, yet the technique has not been extensively utilized to probe colloidal suspensions. Two $Mg(OH)_2$ suspensions were considered due to their considerable differences in sample aging, influenced by dissolution-precipitation mechanisms of MgO conversion to $Mg(OH)_2$ and Ostwald ripening of smaller $Mg(OH)_2$ crystallites. As a result, the Versamag sample with the higher MgO content (Versamag A) exhibited yield stress aging, with the yield stress of a 22 vol% suspension increasing to ~300 Pa in 70 h, while Versamag B showed minimal yield stress aging and a maximum yield stress of 73.5 Pa. When the QCM sensor was submerged in 22 vol% suspensions, the sensor resonance properties, frequency and resistance, were able to monitor those differences in yield stress aging, with the resonance frequency and resistance increasing as the particle network stiffened (increased yield stress).

In the absence of sample aging, the solids concentration was increased to enhance suspension yield stress. The air-to-sample responses of the QCM sensor were recorded and the shift in resonance resistance shown to correlate with the suspension yield stress. The frequency response was shown to be more complex and likely influenced by multiple factors such as: i) contact mechanics, ii) suspension viscoelasticity and iii) shear wave penetration depth. Since this is the first study of its kind, the present understanding of the resonance frequency remains poorly understood and is the focus of ongoing research. The research has however demonstrated the applicability of QCM to monitor changes in suspension yield stress, which can be of great value, although the full potential of QCM in characterizing colloidal suspensions is yet to be realized.

Supplementary Information

Gel-point determination of Versamag B using the method described in de Kretser et al.[23]. (Fig. S1); QCM experimental set-up – Stanford Research System QCM200 (Fig. S2); Typical TGA (a) and DSC (b) data for the thermal decomposition of dried Versamag A (Fig. S3).

Author Information

Corresponding Author

* D.H., E-mail: d.harbottle@leeds.ac.uk, T: +44(0) 113 343 4154

Acknowledgements

References

1.   O'Sullivan, C. K.; Guilbault, G. G., Commercial quartz crystal microbalances - theory and applications. Biosensors & Bioelectronics **1999,** 14, 663-670.

2.   Sauerbrey, G., Verwendung Von Schwingquarzen Zur Wagung Dunner Schichten Und Zur Mikrowagung. Z Phys **1959,** 155 (2), 206-222.

3.   Kanazawa, K. K.; Gordon, J. G., II, Frequency of a quartz microbalance in contact with liquid. Anal. Chem. **1985,** 57 (8), 1770-1.

4.   Denolf, G. C.; Haack, L.; Holubka, J.; Straccia, A.; Blohowiak, K.; Broadbent, C.; Shull, K. R., High frequency rheometry of viscoelastic coatings with the quartz crystal microbalance. Langmuir 27 (16), 9873-9.

5.   Martin, S. J.; Granstaff, V. E.; Frye, G. C., Characterization of a Quartz Crystal Microbalance with Simultaneous Mass and Liquid Loading. Anal Chem **1991,** 63 (20), 2272-2281.

6.   Johannsmann, D., Viscoelastic, mechanical, and dielectric measurements on complex samples with the quartz crystal microbalance. Phys Chem Chem Phys **2008,** 10 (31), 4516-4534.

7.   Bruckenstein, S.; Shay, M., Experimental aspects of use of the quartz crystal microbalance in solution. Electrochimica Acta **1985,** 30 (10), 1295-300.

8.   Nomura, T.; Hattori, O., Determination of Micromolar Concentrations of Cyanide in Solution with a Piezoelectric Detector. Anal Chim Acta **1980,** 115 (Mar), 323-326.

9.   Nomura, T.; Okuhara, M., Frequency shifts of piezoelectric quartz crystals immersed in organic liquids. Anal Chim Acta **1982,** 142, 281-284.

10.   Kanazawa, K. K.; Gordon, J. G., II, The oscillation frequency of a quartz resonator in contact with a liquid. Analytica Chimica Acta **1985,** 175, 99-105.

11.   Mason, W. P.; Baerwald, H., Piezoelectric crystals and their applications to ultrasonics. Physics Today **1951,** 4, 23.

12.   Nakamoto, T.; Moriizumi, T., A Theory of a Quartz Crystal Microbalance Based Upon a Mason Equivalent-Circuit. Jpn J Appl Phys 1 **1990,** 29 (5), 963-969.

13.   Voinova, M. V.; Rodahl, M.; Jonson, M.; Kasemo, B., Viscoelastic acoustic response of layered polymer films at fluid-solid interfaces: Continuum mechanics approach. Phys Scripta **1999,** 59 (5), 391-396.

14.   Johannsmann, D.; Reviakine, I.; Richter, R. P., Dissipation in Films of Adsorbed Nanospheres Studied by Quartz Crystal Microbalance (QCM). Anal Chem **2009,** 81 (19), 8167-8176.

15.   Reipa, V.; Purdum, G.; Choi, J., Measurement of nanoparticle concentration using quartz crystal microgravimetry. The Journal of Physical Chemistry B **2010,** 114 (49), 16112-16117.

16.   Fatisson, J.; Domingos, R. F.; Wilkinson, K. J.; Tufenkji, N., Deposition of TiO2 nanoparticles onto silica measured using a quartz crystal microbalance with dissipation monitoring. Langmuir **2009,** 25 (11), 6062-6069.

17.   Gotoh, K.; Nakata, Y.; Tagawa, M., Evaluation of particle deposition in aqueous solutions by the quartz crystal microbalance method. Colloids and Surfaces A: Physicochemical and Engineering Aspects **2006,** 272 (1), 117-123.

18.   Marxer, C. M.; Coen, M. C.; Greber, T.; Greber, U. F.; Schlapbach, L., Cell spreading on quartz crystal microbalance elicits positive frequency shifts indicative of viscosity changes. Anal Bioanal Chem **2003,** 377 (3), 578-586.

19.   Tellechea, E.; Johannsmann, D.; Steinmetz, N. F.; Richter, R. P.; Reviakine, I., Model-Independent Analysis of QCM Data on Colloidal Particle Adsorption. Langmuir **2009,** 25 (9), 5177-5184.

20.   Pomorska, A.; Shchukin, D.; Hammond, R.; Cooper, M. A.; Grundmeier, G.; Johannsmann, D., Positive Frequency Shifts Observed Upon Adsorbing Micron-Sized Solid Objects to a Quartz Crystal Microbalance from the Liquid Phase. Anal Chem **2010,** 82 (6), 2237-2242.

21.   Dybwad, G. L., A sensitive new method for the determination of adhesive bonding between a particle and a substrate. Journal of Applied Physics **1985,** 58 (7), 2789-2790.

22.   Johnson, M.; Peakall, J.; Fairweather, M.; Biggs, S.; Harbottle, D.; Hunter, T. N., Characterization of Multiple Hindered Settling Regimes in Aggregated Mineral Suspensions. Industrial & Engineering Chemistry Research **2016,** 55 (37), 9983-9993.

23.   De Kretser, R. G.; Boger, D. V.; Scales, P. J., Compressive rheology: an overview. Rheology Reviews **2003**, 125-166.

24.   Franks, G. V.; Zhou, Y.; Yan, Y. D.; Jameson, G. J.; Biggs, S., Effect of aggregate size on sediment bed rheological properties. Phys. Chem. Chem. Phys. **2004,** 6 (18), 4490-4498.

25.   Liddell, P. V.; Boger, D. V., Yield stress measurements with the vane. J. Non-Newton. Fluid Mech. **1996,** 63 (2-3), 235-261.

26.   Dzuy, N. Q.; Boger, D. V., Yield Stress Measurement for Concentrated Suspensions. J Rheol **1983,** 27 (4), 321-349.

27.   Alderman, N. J.; Meeten, G. H.; Sherwood, J. D., Vane rheometry of bentonite gels. Journal of Non-Newtonian Fluid Mechanics **1991,** 39 (3), 291-310.

28.   Dzuy, N. Q.; Boger, D. V., Direct Yield Stress Measurement with the Vane Method. J Rheol **1985,** 29 (3), 335-347.

29.   Johnson, S. B.; Franks, G. V.; Scales, P. J.; Boger, D. V.; Healy, T. W., Surface chemistry-rheology relationships in concentrated mineral suspensions. International Journal of Mineral Processing **2000,** 58 (1-4), 267-304.

30.   Zigan, F.; Rothbauer, R., Neutronenbeugungsmessungen am brucit. Neues Jahrbuch für Mineralogie Monatshefte **1967,** 1967, 137À143.

31.   Anderson, P. J.; Horlock, R. F., Thermal Decomposition of Magnesium Hydroxide. T Faraday Soc **1962,** 58 (478), 1993-&.

32.   Johannsmann, D., The Quartz Crystal Microbalance in Soft Matter Research. Springer: 2014.

33.   Langford, J. I.; Wilson, A., Scherrer after sixty years: a survey and some new results in the determination of crystallite size. Journal of Applied Crystallography **1978,** 11 (2), 102-113.

34.   Mullin, J. W.; Murphy, J. D.; Sohnel, O.; Spoors, G., Aging of Precipitated Magnesium-Hydroxide. Ind Eng Chem Res **1989,** 28 (11), 1725-1730.

35.   Halikia, I.; Neou-Syngouna, P.; Kolitsa, D., Isothermal kinetic analysis of the thermal decomposition of magnesium hydroxide using thermogravimetric data. Thermochim Acta **1998,** 320 (1-2), 75-88.

36.   Sinelnikov, S.; Gropyanov, V., Kinetics of non-isothermal decomposition of magnesium-hydroxide. J Appl Chem-Ussr+ **1982,** 55 (3), 461-463.

37.   Thomas, J. J.; Musso, S.; Prestini, I., Kinetics and Activation Energy of Magnesium Oxide Hydration. J Am Ceram Soc **2014,** 97 (1), 275-282.

38.   Gursky, J. A.; Blough, S. D.; Luna, C.; Gomez, C.; Luevano, A. N.; Gardner, E. A., Particle−Particle Interactions between Layered Double Hydroxide Nanoparticles. Journal of the American Chemical Society **2006,** 128 (26), 8376-8377.

39.   Stumm, W.; Morgan, J., The surface chemistry of oxides, hydroxides, and oxide mineral. Aquatic Chemistry **1981**, 625-640.

40.   Rahnemaie, R.; Hiemstra, T.; van Riemsdijk, W. H., Inner-and outer-sphere complexation of ions at the goethite–solution interface. J Colloid Interf Sci **2006,** 297 (2), 379-388.

41.   Zhang, H.; Yu, K.; Cayre, O. J.; Harbottle, D., Interfacial particle dynamics: One and two step yielding in colloidal glass. Langmuir **2016,** 32 (50), 13472-13481.